

# SCALING PROPERTIES OF DIFFUSION MODELS FOR PERCEPTUAL TASKS

Rahul Ravishankar\*, Zeeshan Patel\*, Jathushan Rajasegaran, Jitendra Malik

University of California, Berkeley

{rravishankar, zeeshanp}@berkeley.edu

## ABSTRACT

In this paper, we argue that iterative computation with diffusion models offers a powerful paradigm for not only generation but also visual perception tasks. We unify tasks such as depth estimation, optical flow, and segmentation under image-to-image translation, and show how diffusion models benefit from scaling training and test-time compute for these perception tasks. Through a careful analysis of these scaling behaviors, we present various techniques to efficiently train diffusion models for visual perception tasks. Our models achieve improved or comparable performance to state-of-the-art methods using significantly less data and compute. We release code and models at [scaling-diffusion-perception.github.io](https://scaling-diffusion-perception.github.io).

## 1 INTRODUCTION

Diffusion and autoregressive models have emerged as powerful techniques for generating images and videos, while showing excellent scaling behaviors. One could attribute part of the success of diffusion models to iterative computation. At inference, diffusion models perform iterative denoising, consuming approximately one to two orders of magnitude more compute compared to a single forward pass.

In this work, we explore how to efficiently scale diffusion model training and inference for downstream perceptual tasks (inverse problems). Marigold (Ke et al., 2024) and FlowDiffuser (Luo et al., 2024) partially answered this question for depth estimation and optical flow individually, showing that diffusion models are indeed suited for such perceptual tasks. Our work explores how to unify a wide range of perceptual tasks, from low-level optical flow to mid-level depth estimation and high-level semantic segmentation / occlusion reasoning, through a detailed study on train/test-time compute scaling behavior.

To study the scaling properties of diffusion models for inverse problems both at training and test-time, we pre-train various dense and mixture-of-expert models for class-conditional image generation. Then, we fine-tune these pre-trained models on downstream perception tasks. We study scaling properties of fine-tuning by varying model size, data resolution, and pre-training compute. In addition, we apply efficient training strategies such as upcycling dense checkpoints to mixture-of-experts models. We also experiment with various test-time compute scaling techniques, including increasing diffusion steps, test-time ensembling, increasing active model experts, and reorganizing compute with noise variance schedules.

We display the effectiveness of leveraging iterative feedback computation through diffusion models for visual perception tasks with three key contributions:

- We perform an *in-depth study of train/test-time compute scaling laws across all layers of the stack*, including pre-training, fine-tuning, and diffusion inference. Specifically, we perform our study on the monocular depth estimation task.
- We show how to *transfer the scaling laws* derived for depth estimation to boost performance on tasks such as optical flow or amodal segmentation for both training and inference.
- We apply all of our scaling strategies to efficiently *train a generalist mixture-of-experts model* on perception tasks, achieving state-of-the-art results across various benchmarks.

---

\*Equal Contribution

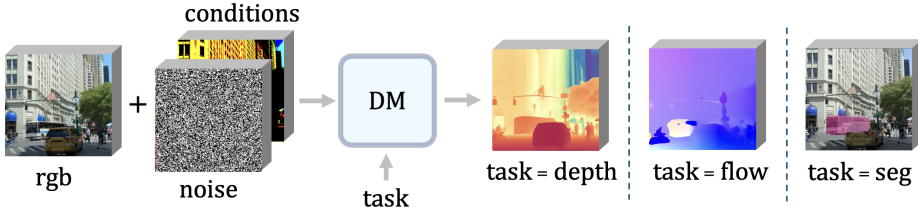


Figure 1: **A Unified Framework:** We fine-tune a pre-trained Diffusion Model (DM), for visual perception tasks. We take a RGB image, and a conditional image (i.e. next video frame, occlusion mask, etc.), along with the noised image of the ground truth prediction. Our model generates predictions for various visual tasks such as monocular depth estimation, optical flow prediction, and amodal segmentation / completion, based on the conditional task embedding. We train one generalist model that can perform all three tasks with exceptional performance.

## 2 RELATED WORK

**Generative Modeling:** Generative modeling has been studied under various methods, including VAEs (Kingma, 2013), GANs (Goodfellow et al., 2014), Normalizing Flows (Rezende & Mohamed, 2015), Autoregressive models (van den Oord et al., 2016), and Diffusion models (Sohl-Dickstein et al., 2015; Ho et al., 2020). Denoising Diffusion Probabilistic Models (DDPMs) (Ho et al., 2020) have shown impressive scaling behaviors, becoming the de facto generative tool for many image and video generation models. Notable examples include Latent Diffusion Models (Rombach et al., 2022), which enhanced efficiency by operating in a compressed latent space, Imagen (Saharia et al., 2022), which generates samples in pixel space with increasing resolution, and Consistency Models (Song et al., 2023), which aim to accelerate sampling while maintaining generation quality. Recent methods like Rectified Flow (Liu et al., 2022) and Flow Matching (Lipman et al., 2023) employ training objectives inspired by optimal transport to model continuous vector fields that map data to target distributions, eliminating the discrete steps typical in diffusion models. Rectified Flow mitigates numerical issues in training by applying flow regularization, and Flow Matching offers efficient sampling with fewer discretization artifacts, making them promising alternatives to diffusion-based approaches for high-quality generation. Apart from diffusion models, Parti (Yu et al., 2022) and MARS (He et al., 2024) showcased the potential of autoregressive models for image generation, and the Muse architecture (Chang et al., 2023) introduced a masked image generation approach using transformers.

**Scaling Diffusion Models:** Diffusion modeling has shown impressive scaling behaviors in terms of data, model size, and compute. Latent Diffusion Models (Rombach et al., 2022) first showed that training with large-scale web datasets can achieve high quality image generation results with a U-Net backbone. DiT (Peebles & Xie, 2023) explored scaling diffusion models with the transformer architecture, presenting desirable scaling properties for class-conditional image generation. Later, Li et al. (Li et al., 2024) studied alignment scaling laws of text-to-image diffusion models. Recently, Fei et al. (Fei et al., 2024a) trained mixture-of-experts DiT models up to 16B parameters, achieving high-quality image generation results. Upcycling is another way to scale transformer models. Komatsuzaki et al. (Komatsuzaki et al., 2022) used upcycling to convert a dense transformer-based language model to a mixture-of-experts model without pre-training from scratch. Similarly, EC-DiT Sun et al. (2024) explores how to exploit heterogeneous compute allocation in mixture-of-experts training for DiT models through expert-choice routing and learning to adaptively optimize the compute allocated to specific text-image data samples.

**Diffusion Models for Perception Tasks:** Diffusion models have also been used for various downstream visual tasks such as depth estimation (Ji et al., 2023; Duan et al., 2023; Saxena et al., 2023; 2024; Zhao et al., 2023). More recently, Marigold (Ke et al., 2024) and GeoWizard (Fu et al., 2024) displayed impressive results by repurposing pre-trained diffusion models for monocular depth estimation. Diffusion models with few modifications are used for semantic segmentation for categorical distributions (Hoogeboom et al., 2021; Brempong et al., 2022; Tan et al., 2022; Amit et al., 2021; Baranchuk et al., 2021; Wolleb et al., 2022), instance segmentation (Gu et al., 2024), and panoptic segmentation (Chen et al., 2023). Diffusion models are also used for optical flow (Luo et al., 2024; Saxena et al., 2024) and 3D understanding (Liu et al., 2023; Jain et al., 2022; Poole et al., 2022; Wang et al., 2023; Watson et al., 2022).

### 3 GENERATIVE PRE-TRAINING

We first explore how to efficiently scale diffusion model pre-training. We pre-train diffusion models for class-conditional image generation using a diffusion transformer (DiT) backbone and follow the original model training recipe (Peebles & Xie, 2023).

Starting with a target RGB image  $I \in \mathbb{R}^{u \times u \times 3}$ , where the resolution of the image is  $u \times u$ , our pretrained, frozen Stable Diffusion variational autoencoder (Rombach et al., 2022) compresses the target to a latent  $z_0 \in \mathbb{R}^{w \times w \times 4}$ , where  $w = u/8$ . Gaussian noise is added at sampled time steps to obtain a noisy target latent. Noisy samples are generated as:

$$z_t = \sqrt{\alpha_t} \cdot z_0 + \sqrt{1 - \alpha_t} \cdot \epsilon_t \quad (1)$$

for timestep  $t$ . The noise is distributed as  $\epsilon \sim \mathcal{N}(0, I)$ ,  $t \sim \text{Uniform}(T)$ , with  $T = 1000$  and  $\alpha_t := \prod_{s=1}^t (1 - \beta_s)$ , with  $\{\beta_1, \dots, \beta_T\}$  as the variance schedule of a process.

In the denoising process, the class-conditional DiT  $f_\theta(\cdot)$ , parameterized by learned parameters  $\theta$ , gradually removes noise from  $z_t$  to obtain  $z_{t-1}$ . The parameters  $\theta$  are updated by noising  $z_0$  with sampled noise  $\epsilon$  at a random timestep  $t$ , computing the noise estimate, and optimizing the mean squared loss between the generated noise and estimated noise in an  $n$  batch size sample. We formally represent this as the following minimization problem:

$$\theta^* = \arg \min_{\theta} \mathcal{L}_\theta(z_t, \epsilon_i) = \arg \min_{\theta} \frac{1}{n} \sum_{i=1}^n (\epsilon_i - \hat{\epsilon}_i)^2, \quad (2)$$

where  $\theta^*$  are the DiT learned parameters and  $\hat{\epsilon}_i$  is the DiT noise prediction for sample  $i$ .

#### 3.1 MODEL SIZE

We pre-train six different dense DiT models as in Table 1, increasing model size by varying the number of layers and hidden dimension size. We use Imagenet-1K (Russakovsky et al., 2015) as our pre-training dataset and train all models for 400k iterations with a fixed learning rate of  $1e-4$  and a batch size of 256. Fig. 2 shows that larger models converge to lower loss with a clear power law scaling behavior. We show the train loss as a function of compute (in MACs), and our predictions indicate a power law relationship of  $L(C) = 0.23 \times C^{-0.0098}$ . Our pre-training experiments display the ease of scaling DiT with a small training dataset, which translates directly to efficiently scaling downstream model performance.

#### 3.2 MIXTURE OF EXPERTS

We also pre-train Sparse Mixture of Experts (MoE) models (Shazeer et al., 2017), following the S/2 and L/2 model configurations in (Fei et al., 2024b). We use three different MoE configurations listed in Table 2, scaling the total parameter count by increasing hidden size, number of experts, layers, and attention heads. Each MoE block activates the top-2 experts per token and has a shared expert that is used by all tokens. To alleviate issues with expert balance, we use the proposed expert balance loss function from (Fei et al., 2024b) which distributes the load across experts more efficiently. Sparse MoE pre-training allows for a higher parameter count while increasing throughput, making it more compute efficient than training a dense DiT model of the same size. We train our DiT-MoE models with the same training recipe as the dense DiT model using ImageNet-1K. Our approach enables training DiT-MoE models to increase model capacity without increasing compute usage by another order of magnitude, which would be required to train dense models of similar sizes.

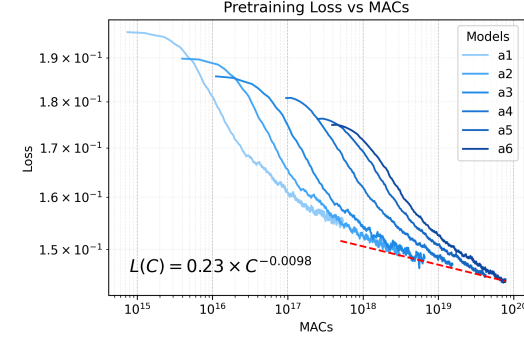


Figure 2: **Scaling at Model Size:** For generative pre-training of DiT models, we observe clear power law scaling behavior as we increase the model size.

Model	Params	Dimension	Heads	Layers
a1	14.8M	256	16	12
a2	77.2M	512	16	16
a3	215M	768	16	20
a4	458M	1024	16	24
a5	1.2B	1536	16	28
a6	1.9B	1792	16	32

Table 1: **Dense DiT Models:** We scale dense DiT model size by increasing hidden dimension and number of layers linearly while keeping number of heads constant following (Yang et al., 2022; Touvron et al., 2023; ?).

Model	Active / Total	Dim	Heads	Layers
S/2-8E2A	71M / 199M	384	6	12
S/2-16E2A	71M / 369M	384	6	12
L/2-8E2A	1.0B / 2.8B	1024	16	24

Table 2: **MoE DiT Models:** We scale the MoE DiT models by increasing dimension size, number attention heads, layers, and experts following (Fei et al., 2024b).

## 4 FINE-TUNING FOR PERCEPTUAL TASKS

In this section, we explore how to scale the fine-tuning of the pre-trained DiT models to maximize performance on downstream perception tasks. During fine-tuning, we utilize the image-to-image diffusion process from (Ke et al., 2024) and (Brooks et al., 2023) as our training recipe. We pose all our visual tasks as conditional denoising diffusion generation. Give an RGB image  $I \in \mathbb{R}^{u \times u \times 3}$  and its pair ground truth image  $D \in \mathbb{R}^{u \times u \times 3}$ , we first project them to the latent space,  $i_0 \in \mathbb{R}^{w \times w \times 4}$  and  $d_0 \in \mathbb{R}^{w \times w \times 4}$ , respectively. We only add noise to the ground truth latent to obtain  $d_t$  and concatenate it with the RGB latent which results in a tensor  $z_t = \{i_0, d_t\}$ . The first convolutional layer of the DiT model is modified to match the doubled number of input channels, and its values are reduced by half to make sure the predictions are the same if the inputs are just RGB images (Ke et al., 2024). Finally, we perform diffusion training by denoising the ground truth image. We ablate several fine-tuning compute scaling techniques on the monocular depth estimation task and report Absolute Relative error and Delta1 error. We transfer the best configurations from the depth estimation ablation study to fine-tune for other visual perception tasks.

### 4.1 EFFECT OF MODEL SIZE

We fine-tune the pre-trained a1-a6 dense models on the depth estimation task to study the effect of model size. We scale model size as shown in as described in Section 3.1. Fig. 3 shows that larger dense DiT models predictably converge to a lower fine-tuning loss, presenting a clear power law scaling behavior. We plot the train loss and validation metrics as a function of compute (in MACs). Our fine-tuned model predictions show a power law relationship in both depth Absolute Relative error and depth Delta1 error. These experiments provide strong signal on how model performance will scale as we increase fine-tuning compute by scaling model size.

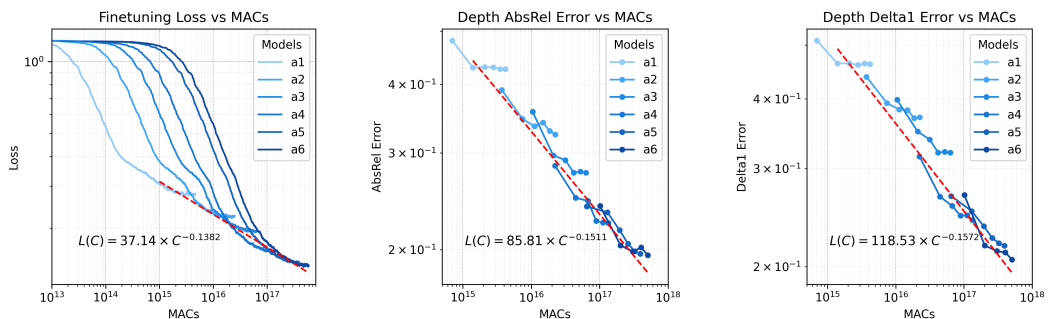
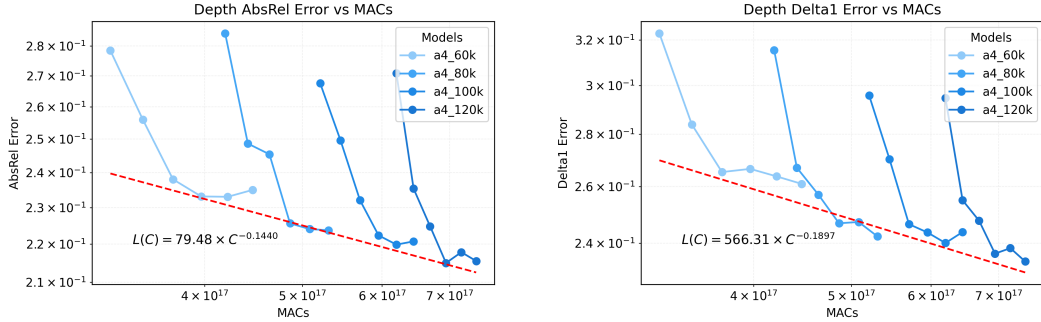


Figure 3: **Effect of Model Size:** We fine-tune a1-a6 models on the Hypersim dataset for 30K iterations with an exponential decay learning rate schedule from  $3e-5$  to  $3e-7$ . We observe a strong correlation between the fine-tuning loss scaling law and validation metric scaling laws.

## 4.2 EFFECT OF PRE-TRAINING COMPUTE

We also investigate the behavior of fine-tuning as we scale the number of pre-training steps for the DiT backbone. We train four models with the a4 configuration using a varied number of pre-training steps, keeping all other hyperparameters constant. We then fine-tune these four models on the same depth estimation dataset. Fig. 4 displays the power law scaling behavior of the validation metrics for depth estimation as we increase DiT pre-training steps. Our experiments show that having stronger pre-trained representations can be helpful when scaling fine-tuning compute.



**Figure 4: Effect of Scaling Model Pre-training Compute on Depth Estimation:** (a) Depth Absolute Relative Error vs. MACs. (b) Depth Delta1 Error vs. MACs. We pre-train four a4 models with 60K, 80K, 100K, and 120K steps. These models are then fine-tuned for 30K steps on the Hypersim depth estimation dataset. We observe a clear power law as we increase the DiT pre-training compute across depth estimation validation metrics.

## 4.3 EFFECT OF IMAGE RESOLUTION

The sequence length of each image also affects the total compute spent during training. For each forward pass, we can scale the amount of compute used by simply increasing the resolution of the image, which will increase the number of tokens in the image embedding. By increasing the number of tokens, we can increase the amount of information the model can learn from at training time to build stronger internal representations, which can in turn improve downstream performance. We use dense DiT-XL models with resolutions of  $256 \times 256$  and  $512 \times 512$  from (Peebles & Xie, 2023) and we pre-train DiT-MoE L/2-8E2A models with  $256 \times 256$  and  $512 \times 512$  resolutions following the recipe in (Fei et al., 2024b). We then fine-tune each of these models with the corresponding resolution for the depth estimation task. Fig. 5 displays that increasing image resolution to scale fine-tuning compute can provide significant gains on downstream depth estimation performance.

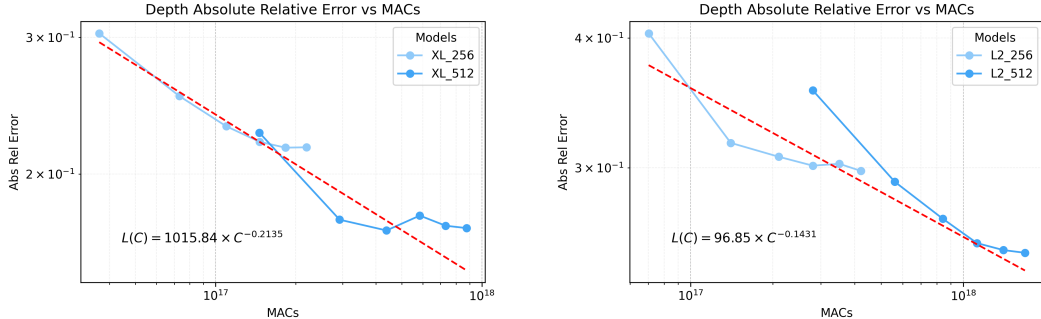


**Figure 5: Effect of Image Resolution.** We fine-tune DiT-XL and DiT-MoE L/2 models with resolutions of  $256 \times 256$  and  $512 \times 512$ . We observe a power law when increasing image resolution during training. By scaling the number of tokens per image by 4 $\times$ , we achieve strong performance on Depth Absolute Error, displaying the effect of increasing total dataset tokens for dense visual perception tasks such as depth estimation.

#### 4.4 EFFECT OF UPCYCLING

Sparse MoE models are efficient options for increasing the capacity of a model, but pre-training an MoE model from scratch can be expensive. One way to alleviate this issue is Sparse MoE Upcycling (Komatsuzaki et al., 2023). Upcycling converts a dense transformer checkpoint to an MoE model by copying the MLP layer in each transformer block  $E$  times, where  $E$  is the number of experts, and adding a learnable router module that sends each token to the top- $k$  selected experts. The outputs of the selected experts are then combined in a weighted sum at the end of each MoE block. We upcycle various dense DiT models after they are fine-tuned for depth estimation and then continue fine-tuning the upcycled model. Fig. 6 displays the scaling laws for upcycling, providing an average improvement of 5.3% on Absolute Relative Error and 8.6% on Delta1 error.

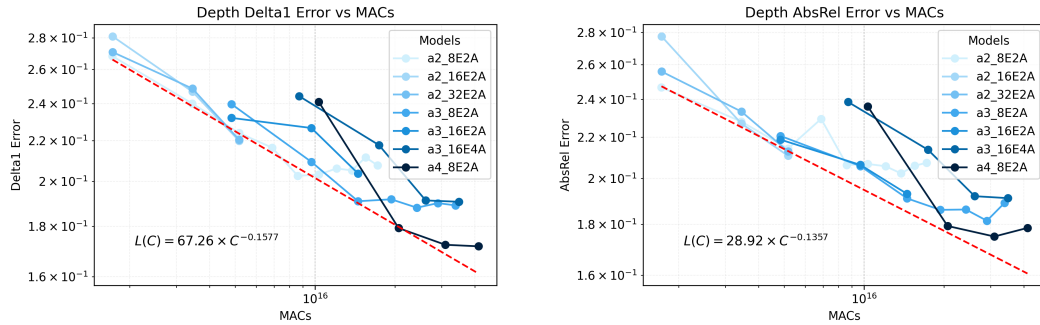


Figure 6: **Effect of Upcycling.** We upcycle a2, a3, and a4 models fine-tuned for depth estimation with a varying number of total/active model experts. We continue fine-tuning each upcycled model for 15K iterations on the Hypersim depth estimation dataset. We observe a clear scaling law in the validation metrics as we increase fine-tuning compute with upcycling. The upcycled models can also achieve equivalent or superior performance to our dense a5 and a6 checkpoints, each of which utilize more compute during pre-training and fine-tuning. Increasing the total model experts and total active experts can also improve the downstream performance.

#### 5 SCALING TEST-TIME COMPUTE

Scaling test-time compute has been explored for autoregressive Large Language Models (LLMs) to improve performance on long-horizon reasoning tasks (Brown et al., 2024; Snell et al., 2024; El-Refai et al., 2024; OpenAI, 2024). In this section, we show how to reliably improve diffusion model performance for perceptual tasks by scaling test-time compute. We summarize our approach in Fig. 7. We use the Stable-Diffusion VAE to encode the input image into latent space (Rombach et al., 2022). Then, we sample a target noise latent from a standard Gaussian distribution, which is iteratively denoised with DDIM (Song et al., 2021) to generate the downstream prediction.

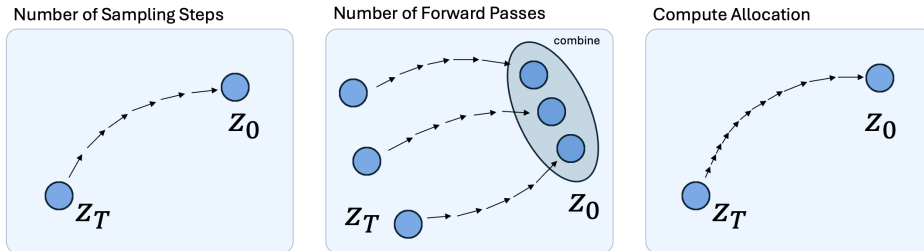


Figure 7: **Inference Scaling:** Diffusion models by design allow efficient scaling of test-time compute. First, we can simply increase the number of denoising steps to increase the compute spent at inference. Since we are estimating deterministic outputs, we can then initialize multiple noise latents and ensemble the predictions to get a better estimation. Finally, we can also reallocate our test-time compute budget for low and high frequency denoising by modifying the noise variance schedule.

### 5.1 EFFECT OF SCALING INFERENCE STEPS

The most natural way of scaling diffusion inference is by increasing denoising steps. Since the model is trained to denoise the input at various timesteps, we can scale the number of diffusion denoising steps at test-time to produce finer, more accurate predictions. This coarse-to-fine denoising paradigm is also reflected in the generative case, and we can take advantage of it for the discriminative case by increasing the number of denoising steps. In Fig. 8, we observe that increasing the total test-time compute by simply increasing the number of diffusion sampling steps provides substantial gains in depth estimation performance.

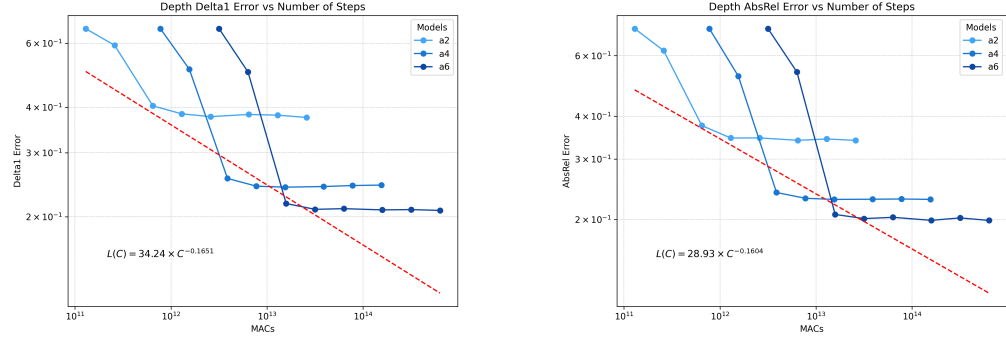


Figure 8: **Effect of Number of Sampling Steps.** (a) Delta1 Error vs. Number of Steps. (b) Absolute Relative Error vs. Number of Steps. For each model, we sample for  $T \in [1, 2, 5, 10, 20, 50, 100]$  steps with the DDIM sampler. We show a clear power law scaling behavior in (a) and (b), displaying the effectiveness of scaling test-time compute by increasing the number of diffusion sampling steps.

### 5.2 EFFECT OF TEST TIME ENSEMBLING

We also explore scaling inference compute with test-time ensembling. We exploit the fact that denoising different noise latents will generate different downstream predictions. In test-time ensembling, we compute  $N$  forward passes for each input sample and reduce the outputs through one of two methods. The first technique is naive ensembling where we use the pixel-wise median across all outputs as the prediction. The second technique presented in Marigold (Ke et al., 2024) is median compilation, where we collect predictions  $\{\hat{d}_1, \dots, \hat{d}_N\}$  that are affine-invariant, jointly estimate scale and shift parameters  $\hat{s}_i$  and  $\hat{t}_i$ , and minimize the distances between each pair of scaled and shifted predictions  $(\hat{d}'_i, \hat{d}'_j)$  where  $\hat{d}' = \hat{d} \times \hat{s} + \hat{t}$ . For each optimization step, we take the pixel-wise median  $\mathbf{m}(x, y) = \text{median}(\hat{d}'_1(x, y), \dots, \hat{d}'_N(x, y))$  to compute the merged depth  $\mathbf{m}$ . Since it requires no ground truth, we scale ensembling by increasing  $N$  to utilize more test-time compute.

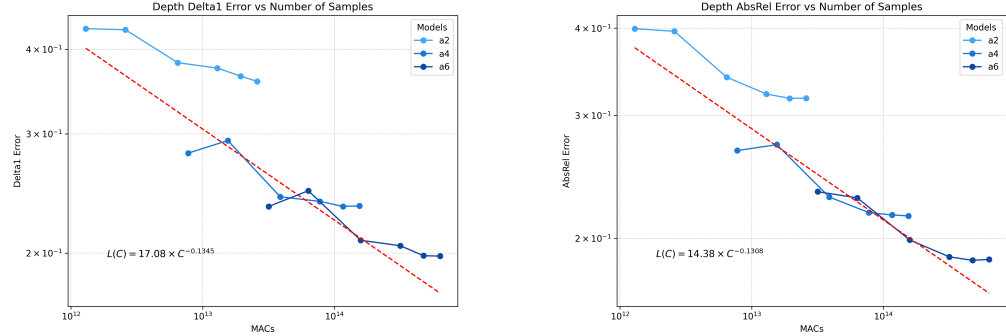


Figure 9: **Effect of Test Time Ensembling.** (a) Depth Delta1 Error vs. Number of Forward Passes. (b) Depth AbsRel Error vs. Number of Forward Passes. Ensembling multiple predictions from distinct noise initializations displays power law scaling behavior. We apply test-time ensembling values of  $N \in [1, 2, 5, 10, 15, 20]$ .

### 5.3 EFFECT OF NOISE VARIANCE SCHEDULE

We can also scale test-time compute by increasing compute usage at different points of the denoising process. In diffusion noise schedulers, we can define a schedule for the variance of the Gaussian noise applied to the image over the total diffusion timesteps  $T$ . Tuning the noise variance schedule allows for reorganizing compute by allocating more compute to denoising steps earlier or later in the noise schedule. We experiment with three different noise level settings for DDIM: linear, scaled linear, and cosine. Cosine scheduling from (Nichol & Dhariwal, 2021) linearly declines from the middle of the corruption process, ensuring the image is not corrupted too quickly as in linear schedules. Fig. 10 shows that the cosine noise variance schedule outperforms linear schedules for DDIM on the depth estimation task under a fixed compute budget.

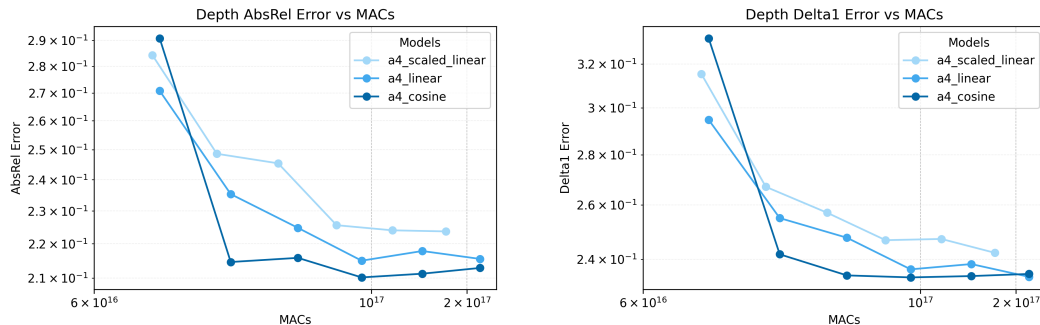


Figure 10: **Effect of Noise Variance (Beta) Schedule.** We fine-tune a4 models with three different beta schedules: linear, scaled linear, cosine. Reallocationing compute with the cosine schedule to spend more time denoising at earlier timesteps significantly improved Delta1 and Absolute Relative Error rates.

## 6 PUTTING IT ALL TOGETHER

Using the lessons from our scaling experiments on depth estimation, we train diffusion models for optical flow prediction and amodal segmentation. We show that using diffusion models while considering efficient methods to scale training and test-time compute can provide substantial performance gains on visual perception tasks, achieving improved or similar performance as current state-of-the-art techniques. Our experiments provide insight on how to efficiently apply diffusion models for these visual perception tasks under limited compute budgets. Finally, we train a unified expert model, capable of performing all three visual perception tasks previously mentioned, displaying the generalizability of our method. Our results prove the effectiveness of our training and test-time scaling strategies, removing the need to use pre-trained models trained on internet-scale datasets to enable high-quality visual perception in diffusion models. Fig. 11 displays the predicted samples from our models.

### 6.1 DEPTH ESTIMATION

We combine our findings from the ablation studies on depth estimation to create a model with the best training and inference configurations. We train a DiT-XL model from (Peebles & Xie, 2023) on depth estimation data from Hypersim for 30K steps with a batch size of 1024, resolution of  $512 \times 512$ , and a learning rate exponentially decaying from  $1.2e-4$  to  $1.2e-6$ . We use median compilation ensembling with a cosine noise variance schedule. From our scaling experiments, we found the optimal configuration for inference to be 200 denoising steps with  $N = 5$  samples for ensembling. As shown in Table 3, our model achieves the same validation performance as Marigold on the Hypersim dataset, while being trained with lower resolution images and approximately **three orders of magnitude less pre-training data and compute**.

Method	Hypersim		ETH3D		NYUv2		ScanNet		DIODE	
	AbsRel $\downarrow$	$\delta 1 \uparrow$								
DiverseDepth	—	—	22.8	69.4	11.7	87.5	10.9	88.2	37.6	63.1
MiDaS	—	—	18.4	75.2	11.1	88.5	12.1	84.6	33.2	71.5
LeReS	—	—	17.1	77.7	9.0	91.6	9.1	91.7	27.1	76.6
Omnidata	—	—	16.6	77.8	7.4	94.5	7.5	93.6	33.9	74.2
HDN	—	—	12.1	83.3	6.9	94.8	8.0	93.9	24.6	78.0
DPT	—	—	7.8	94.6	9.8	90.3	8.2	93.4	18.2	75.8
Marigold	13.5	87.5	6.5	96.0	5.5	96.4	6.4	95.1	30.8	77.3
<b>Ours</b>	13.6	87.6	4.8	97.8	6.8	95.0	7.7	93.7	31.0	77.2

Table 3: **Depth Estimation Performance Comparison on Multiple Datasets.** We achieve state-of-the-art performance on the ETH3D dataset and competitive performance across all other benchmarks. Notably, we closely match the performance of Marigold across all datasets with significantly less training compute.

## 6.2 OPTICAL FLOW PREDICTION

Optical flow estimation involves predicting the motion of objects between consecutive frames in a video, represented as a dense vector field indicating pixel-wise displacement. We use a similar configuration as the depth estimation model for optical flow training. We train a DiT-XL model on the FlyingChairs dataset for 40K steps with batch size of 1024, resolution of  $512 \times 512$ , and learning rate exponentially decaying from  $1.2e-4$  to  $1.2e-6$ . We compare our model’s performance with other specialized optical flow prediction techniques in Table 4.

Method	FlyingChairs EPE $\downarrow$
DeepFlow	3.53
FlowNetS	2.71
FlowNetS+v	2.86
FlowNetS+ft	3.04
FlowNetS+ft+v	3.03
FlowNetC	2.19
FlowNetC+v	2.61
FlowNetC+ft	2.27
FlowNetC+ft+v	2.67
<b>Ours (w/o ensembling)</b>	3.45
<b>Ours (w/ ensembling)</b>	3.08

Table 4: **Optical Flow Comparison with Specialized Techniques.** We evaluate our optical flow model on the FlyingChairs validation set. Our model achieves similar endpoint error as specialized methods, including DeepFlow (Weinzaepfel et al., 2013) and FlowNet (Fischer et al., 2015). We train with significantly less data compared to other specialized methods, which use a several optical flow datasets. We generate predictions with and without test-time ensembling.

## 6.3 AMODAL SEGMENTATION

Amodal segmentation is the process of predicting the complete shape and extent of objects in an image, including the portions that are occluded or not directly visible, which can require higher-level reasoning for complex scenes. We fine-tune a DiT-XL model on the pix2gestalt dataset (Ozguroglu et al., 2024) for 6K steps with a batch size of 4096, resolution of  $256 \times 256$ , and learning rate exponentially decaying from  $1.2e-4$  to  $1.2e-6$ . We compare our model with other methods in Table 5.

Method	COCO-A	P2G	MP3D
PCNet	81.35	—	—
PCNet-Sup	82.53	—	—
SAM	67.21	—	—
SD-XL Inpainting	76.52	—	—
Pix2Gestalt	82.9	88.7	61.5
<b>Ours</b>	82.9	88.6	63.9

Table 5: **Amodal Segmentation Performance (mIOU) Comparison Across Different Datasets.** This table compares mIOU performance across COCO-A, Pix2Gestalt, and MP3D datasets, showing the effectiveness of various methods. Our method is able to achieve competitive performance across all tasks, while training only on Pix2Gestalt.

#### 6.4 ONE MODEL FOR ALL

We train a unified DiT-XL model for each of the different tasks. We train this model on a mixed dataset consisting of all three tasks. To train this generalist model, we modify the DiT-XL architecture by replacing the patch embedding layer with a separate `PatchEmbedRouter` module, which routes each VAE embedding to a specific input convolutional layer based perception task. This ensures the DiT-XL model is able to distinguish between the task-specific embeddings during fine-tuning. We use a similar training recipe as the previous experiments, using images with  $512 \times 512$  resolution and a learning rate exponentially decaying from  $1.2e-4$  to  $1.2e-6$ . Then, we upcycle the fine-tuned DiT-XL checkpoint to an DiT-XL-8E2A model, and continue fine-tuning for another 4K iterations. We display the generated predictions in Fig. 11 which exemplify the generalizability and transferability of our scaling techniques across a variety of perception tasks.

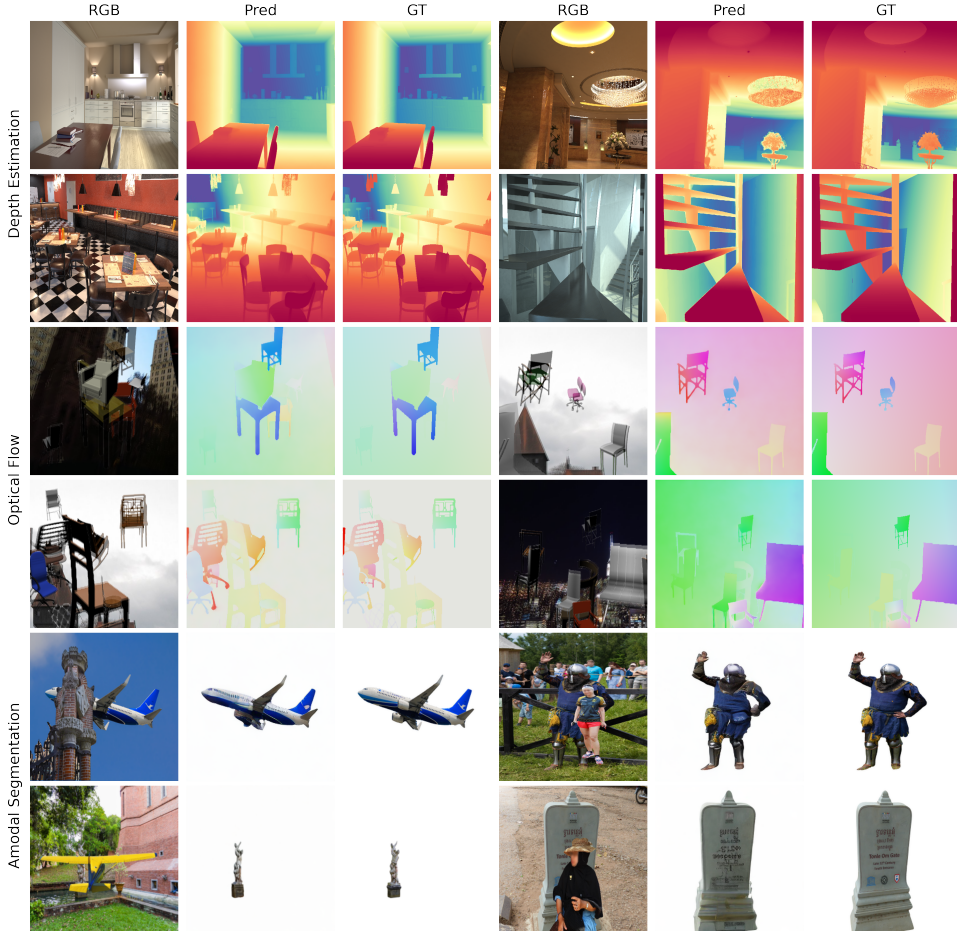


**Figure 11: Depth Estimation, Optical Flow Estimation, and Amodal Segmentation Examples:** Each row showcases results from our models for different tasks. (a) Depth estimation, with relative scale and shift. (b) Optical flow, with scale and shift. (c) Amodal segmentation, where the model sees an RGB image and segmentation of the occluded object; the task is to predict the amodal image.

## 7 CONCLUSION

In our work, we examine the scaling properties of diffusion models for visual perception tasks. We explore various approaches to scale diffusion training, including increasing model size, mixture-of-experts models, increasing image resolution, and upcycling. We also efficiently scale test-time compute by exploiting the iterative nature of diffusion, which significantly improves downstream performance. Our experiments provide strong evidence of scaling, uncovering power laws across various training and inference scaling techniques. We hope to inspire future work in scaling training and test-time compute for iterative generative paradigms such as diffusion for perception tasks.

## 8 ACKNOWLEDGMENTS

We thank Alexei Efros for helpful discussions. We also thank Xinlei Chen, Amil Dravid, Neerja Thakkar for their valuable feedback on the paper.

## REFERENCES

Tomer Amit, Tal Shahrabany, Eliya Nachmani, and Lior Wolf. Segdiff: Image segmentation with diffusion probabilistic models. *arXiv preprint arXiv:2112.00390*, 2021.

Dmitry Baranchuk, Ivan Rubachev, Andrey Voynov, Valentin Khrulkov, and Artem Babenko. Label-efficient semantic segmentation with diffusion models. *arXiv preprint arXiv:2112.03126*, 2021.

Emmanuel Asiedu Brempong, Simon Kornblith, Ting Chen, Niki Parmar, Matthias Minderer, and Mohammad Norouzi. Denoising pretraining for semantic segmentation. In *Proceedings of the IEEE/CVF conference on computer vision and pattern recognition*, pp. 4175–4186, 2022.

Tim Brooks, Aleksander Holynski, and Alexei A. Efros. Instructpix2pix: Learning to follow image editing instructions, 2023. URL <https://arxiv.org/abs/2211.09800>.

Bradley Brown, Jordan Juravsky, Ryan Ehrlich, Ronald Clark, Quoc V. Le, Christopher Ré, and Azalia Mirhoseini. Large language monkeys: Scaling inference compute with repeated sampling, 2024. URL <https://arxiv.org/abs/2407.21787>.

Huiwen Chang, Han Zhang, Jarred Barber, AJ Maschinot, Jose Lezama, Lu Jiang, Ming-Hsuan Yang, Kevin Murphy, William T. Freeman, Michael Rubinstein, Yuanzhen Li, and Dilip Krishnan. Muse: Text-to-image generation via masked generative transformers, 2023. URL <https://arxiv.org/abs/2301.00704>.

Ting Chen, Lala Li, Saurabh Saxena, Geoffrey Hinton, and David J Fleet. A generalist framework for panoptic segmentation of images and videos. In *Proceedings of the IEEE/CVF international conference on computer vision*, pp. 909–919, 2023.

Yiqun Duan, Xianda Guo, and Zheng Zhu. Diffusiondepth: Diffusion denoising approach for monocular depth estimation. *arXiv preprint arXiv:2303.05021*, 2023.

Karim El-Refai, Zeeshan Patel, Jonathan Pei, and Tianle Li. Swag: Storytelling with action guidance, 2024.

Zhengcong Fei, Mingyuan Fan, Changqian Yu, Debang Li, and Junshi Huang. Scaling diffusion transformers to 16 billion parameters. *arXiv preprint arXiv:2407.11633*, 2024a.

Zhengcong Fei, Mingyuan Fan, Changqian Yu, Debang Li, and Jusnshi Huang. Scaling diffusion transformers to 16 billion parameters. *arXiv preprint*, 2024b.

Philipp Fischer, Alexey Dosovitskiy, Eddy Ilg, Philip Häusser, Caner Hazırbaş, Vladimir Golkov, Patrick van der Smagt, Daniel Cremers, and Thomas Brox. Flownet: Learning optical flow with convolutional networks, 2015. URL <https://arxiv.org/abs/1504.06852>.

Xiao Fu, Wei Yin, Mu Hu, Kaixuan Wang, Yuexin Ma, Ping Tan, Shaojie Shen, Dahua Lin, and Xiaoxiao Long. Geowizard: Unleashing the diffusion priors for 3d geometry estimation from a single image, 2024. URL <https://arxiv.org/abs/2403.12013>.

Ian Goodfellow, Jean Pouget-Abadie, Mehdi Mirza, Bing Xu, David Warde-Farley, Sherjil Ozair, Aaron Courville, and Yoshua Bengio. Generative adversarial nets. *Advances in neural information processing systems*, 27, 2014.

Zhangxuan Gu, Haoxing Chen, and Zhuoer Xu. Diffusioninst: Diffusion model for instance segmentation. In *ICASSP 2024-2024 IEEE International Conference on Acoustics, Speech and Signal Processing (ICASSP)*, pp. 2730–2734. IEEE, 2024.

Wanggui He, Siming Fu, Mushui Liu, Xierui Wang, Wenyi Xiao, Fangxun Shu, Yi Wang, Lei Zhang, Zhelun Yu, Haoyuan Li, Ziwei Huang, LeiLei Gan, and Hao Jiang. Mars: Mixture of auto-regressive models for fine-grained text-to-image synthesis, 2024. URL <https://arxiv.org/abs/2407.07614>.

Jonathan Ho, Ajay Jain, and Pieter Abbeel. Denoising diffusion probabilistic models. *Advances in neural information processing systems*, 33:6840–6851, 2020.

Emiel Hoogeboom, Didrik Nielsen, Priyank Jaini, Patrick Forré, and Max Welling. Argmax flows and multinomial diffusion: Learning categorical distributions. *Advances in Neural Information Processing Systems*, 34:12454–12465, 2021.

Ajay Jain, Ben Mildenhall, Jonathan T Barron, Pieter Abbeel, and Ben Poole. Zero-shot text-guided object generation with dream fields. In *Proceedings of the IEEE/CVF conference on computer vision and pattern recognition*, pp. 867–876, 2022.

Yuanfeng Ji, Zhe Chen, Enze Xie, Lanqing Hong, Xihui Liu, Zhaoqiang Liu, Tong Lu, Zhenguo Li, and Ping Luo. Ddp: Diffusion model for dense visual prediction. In *Proceedings of the IEEE/CVF International Conference on Computer Vision*, pp. 21741–21752, 2023.

Bingxin Ke, Anton Obukhov, Shengyu Huang, Nando Metzger, Rodrigo Caye Daudt, and Konrad Schindler. Repurposing diffusion-based image generators for monocular depth estimation. In *Proceedings of the IEEE/CVF Conference on Computer Vision and Pattern Recognition*, pp. 9492–9502, 2024.

Diederik P Kingma. Auto-encoding variational bayes. *arXiv preprint arXiv:1312.6114*, 2013.

Aran Komatsuzaki, Joan Puigcerver, James Lee-Thorp, Carlos Riquelme Ruiz, Basil Mustafa, Joshua Ainslie, Yi Tay, Mostafa Dehghani, and Neil Houlsby. Sparse upcycling: Training mixture-of-experts from dense checkpoints. *arXiv preprint arXiv:2212.05055*, 2022.

Aran Komatsuzaki, Joan Puigcerver, James Lee-Thorp, Carlos Riquelme Ruiz, Basil Mustafa, Joshua Ainslie, Yi Tay, Mostafa Dehghani, and Neil Houlsby. Sparse upcycling: Training mixture-of-experts from dense checkpoints, 2023. URL <https://arxiv.org/abs/2212.05055>.

Hao Li, Yang Zou, Ying Wang, Orchid Majumder, Yusheng Xie, R Manmatha, Ashwin Swaminathan, Zhuowen Tu, Stefano Ermon, and Stefano Soatto. On the scalability of diffusion-based text-to-image generation. In *Proceedings of the IEEE/CVF Conference on Computer Vision and Pattern Recognition*, pp. 9400–9409, 2024.

Y Lipman et al. Flow matching: Symmetrizing optimal transport and generative modeling. *arXiv preprint arXiv:2301.13003*, 2023.

Ruoshi Liu, Rundi Wu, Basile Van Hoorick, Pavel Tokmakov, Sergey Zakharov, and Carl Vondrick. Zero-1-to-3: Zero-shot one image to 3d object. In *Proceedings of the IEEE/CVF international conference on computer vision*, pp. 9298–9309, 2023.

X Liu et al. Rectified flow: A unified approach for free-form generative models. *arXiv preprint arXiv:2209.07953*, 2022.

Ao Luo, Xin Li, Fan Yang, Jiangyu Liu, Haoqiang Fan, and Shuaicheng Liu. Flowdiffuser: Advancing optical flow estimation with diffusion models. In *Proceedings of the IEEE/CVF Conference on Computer Vision and Pattern Recognition*, pp. 19167–19176, 2024.

Alex Nichol and Prafulla Dhariwal. Improved denoising diffusion probabilistic models, 2021. URL <https://arxiv.org/abs/2102.09672>.

OpenAI. Learning to reason with llms. <https://openai.com/index/learning-to-reason-with-llms/>, September 2024.

Ege Ozguroglu, Ruoshi Liu, Dídac Surś, Dian Chen, Achal Dave, Pavel Tokmakov, and Carl Vondrick. pix2gestalt: Amodal segmentation by synthesizing wholes. *Proceedings of the IEEE/CVF Conference on Computer Vision and Pattern Recognition (CVPR)*, 2024.

William Peebles and Saining Xie. Scalable diffusion models with transformers. In *Proceedings of the IEEE/CVF International Conference on Computer Vision*, pp. 4195–4205, 2023.

Ben Poole, Ajay Jain, Jonathan T Barron, and Ben Mildenhall. Dreamfusion: Text-to-3d using 2d diffusion. *arXiv preprint arXiv:2209.14988*, 2022.

Danilo Rezende and Shakir Mohamed. Variational inference with normalizing flows. In *International conference on machine learning*, pp. 1530–1538. PMLR, 2015.

Robin Rombach, Andreas Blattmann, Dominik Lorenz, Patrick Esser, and Björn Ommer. High-resolution image synthesis with latent diffusion models. In *Proceedings of the IEEE/CVF conference on computer vision and pattern recognition*, pp. 10684–10695, 2022.

Olga Russakovsky, Jia Deng, Hao Su, Jonathan Krause, Sanjeev Satheesh, Sean Ma, Zhiheng Huang, Andrej Karpathy, Aditya Khosla, Michael Bernstein, Alexander C. Berg, and Li Fei-Fei. Imagenet large scale visual recognition challenge, 2015. URL <https://arxiv.org/abs/1409.0575>.

Chitwan Saharia, William Chan, Saurabh Saxena, Lala Li, Jay Whang, Emily L Denton, Kamyar Ghasemipour, Raphael Gontijo Lopes, Burcu Karagol Ayan, Tim Salimans, et al. Photorealistic text-to-image diffusion models with deep language understanding. *Advances in neural information processing systems*, 35:36479–36494, 2022.

Saurabh Saxena, Abhishek Kar, Mohammad Norouzi, and David J Fleet. Monocular depth estimation using diffusion models. *arXiv preprint arXiv:2302.14816*, 2023.

Saurabh Saxena, Charles Herrmann, Junhwa Hur, Abhishek Kar, Mohammad Norouzi, Deqing Sun, and David J Fleet. The surprising effectiveness of diffusion models for optical flow and monocular depth estimation. *Advances in Neural Information Processing Systems*, 36, 2024.

Noam Shazeer, Azalia Mirhoseini, Krzysztof Maziarz, Andy Davis, Quoc Le, Geoffrey Hinton, and Jeff Dean. Outrageously large neural networks: The sparsely-gated mixture-of-experts layer, 2017. URL <https://arxiv.org/abs/1701.06538>.

Charlie Snell, Jaehoon Lee, Kelvin Xu, and Aviral Kumar. Scaling llm test-time compute optimally can be more effective than scaling model parameters, 2024. URL <https://arxiv.org/abs/2408.03314>.

Jascha Sohl-Dickstein, Eric Weiss, Niru Maheswaranathan, and Surya Ganguli. Deep unsupervised learning using nonequilibrium thermodynamics. In *International conference on machine learning*, pp. 2256–2265. PMLR, 2015.

Jiaming Song, Chenlin Meng, and Stefano Ermon. Denoising diffusion implicit models. In *International Conference on Learning Representations*, 2021. URL <https://openreview.net/forum?id=St1giarCHLP>.

Yang Song, Prafulla Dhariwal, Mark Chen, and Ilya Sutskever. Consistency models. *arXiv preprint arXiv:2303.01469*, 2023.

Haotian Sun, Tao Lei, Bowen Zhang, Yanghao Li, Haoshuo Huang, Ruoming Pang, Bo Dai, and Nan Du. Ec-edit: Scaling diffusion transformers with adaptive expert-choice routing, 2024. URL <https://arxiv.org/abs/2410.02098>.

Haorui Tan, Sitong Wu, and Jimin Pi. Semantic diffusion network for semantic segmentation. *Advances in Neural Information Processing Systems*, 35:8702–8716, 2022.

Hugo Touvron, Louis Martin, Kevin Stone, Peter Albert, Amjad Almahairi, Yasmine Babaei, Nikolay Bashlykov, Soumya Batra, Prajjwal Bhargava, Shruti Bhosale, Dan Bikel, Lukas Blecher, Cristian Canton Ferrer, Moya Chen, Guillem Cucurull, David Esibou, Jude Fernandes, Jeremy Fu, Wenyin Fu, Brian Fuller, Cynthia Gao, Vedanuj Goswami, Naman Goyal, Anthony Hartshorn, Saghar Hosseini, Rui Hou, Hakan Inan, Marcin Kardas, Viktor Kerkez, Madian Khabsa, Isabel Kloumann, Artem Korenev, Punit Singh Koura, Marie-Anne Lachaux, Thibaut Lavril, Jenya Lee, Diana Liskovich, Yinghai Lu, Yuning Mao, Xavier Martinet, Todor Mihaylov, Pushkar Mishra,

Igor Molybog, Yixin Nie, Andrew Poulton, Jeremy Reizenstein, Rashi Rungta, Kalyan Saladi, Alan Schelten, Ruan Silva, Eric Michael Smith, Ranjan Subramanian, Xiaoqing Ellen Tan, Binh Tang, Ross Taylor, Adina Williams, Jian Xiang Kuan, Puxin Xu, Zheng Yan, Iliyan Zarov, Yuchen Zhang, Angela Fan, Melanie Kambadur, Sharan Narang, Aurelien Rodriguez, Robert Stojnic, Sergey Edunov, and Thomas Scialom. Llama 2: Open foundation and fine-tuned chat models, 2023. URL <https://arxiv.org/abs/2307.09288>.

Aäron van den Oord, Nal Kalchbrenner, and Koray Kavukcuoglu. Pixel recurrent neural networks. In Maria Florina Balcan and Kilian Q. Weinberger (eds.), *Proceedings of The 33rd International Conference on Machine Learning*, volume 48 of *Proceedings of Machine Learning Research*, pp. 1747–1756, New York, New York, USA, 20–22 Jun 2016. PMLR. URL <https://proceedings.mlr.press/v48/oord16.html>.

Haochen Wang, Xiaodan Du, Jiahao Li, Raymond A Yeh, and Greg Shakhnarovich. Score jacobian chaining: Lifting pretrained 2d diffusion models for 3d generation. In *Proceedings of the IEEE/CVF Conference on Computer Vision and Pattern Recognition*, pp. 12619–12629, 2023.

Daniel Watson, William Chan, Ricardo Martin-Brualla, Jonathan Ho, Andrea Tagliasacchi, and Mohammad Norouzi. Novel view synthesis with diffusion models. *arXiv preprint arXiv:2210.04628*, 2022.

Philippe Weinzaepfel, Jerome Revaud, Zaid Harchaoui, and Cordelia Schmid. Deepflow: Large displacement optical flow with deep matching. In *Proceedings of the IEEE International Conference on Computer Vision (ICCV)*, December 2013.

Julia Wolleb, Robin Sandkühler, Florentin Bieder, Philippe Valmaggia, and Philippe C Cattin. Diffusion models for implicit image segmentation ensembles. In *International Conference on Medical Imaging with Deep Learning*, pp. 1336–1348. PMLR, 2022.

Greg Yang, Edward J. Hu, Igor Babuschkin, Szymon Sidor, Xiaodong Liu, David Farhi, Nick Ryder, Jakub Pachocki, Weizhu Chen, and Jianfeng Gao. Tensor programs v: Tuning large neural networks via zero-shot hyperparameter transfer, 2022. URL <https://arxiv.org/abs/2203.03466>.

Jiahui Yu, Yuanzhong Xu, Jing Yu Koh, Thang Luong, Gunjan Baid, Zirui Wang, Vijay Vasudevan, Alexander Ku, Yinfei Yang, Burcu Karagol Ayan, et al. Scaling autoregressive models for content-rich text-to-image generation. *arXiv preprint arXiv:2206.10789*, 2(3):5, 2022.

Wenliang Zhao, Yongming Rao, Zuyan Liu, Benlin Liu, Jie Zhou, and Jiwen Lu. Unleashing text-to-image diffusion models for visual perception. In *Proceedings of the IEEE/CVF International Conference on Computer Vision*, pp. 5729–5739, 2023.